eNeuro

Research Article: New Research | Cognition and Behavior

Neurodynamic Evidence Supports a Forced-Excursion Model of Decision-Making under Speed/Accuracy Instructions

Laure Spieser[1], Carmen Kohl[1], Bettina Forster[1], Sven Bestmann[2] and Kielan Yarrow[1]

[1]*Department of Psychology, Cognitive Neuroscience Research Unit, University of London, London, EC1V 0HB, UK*

[2]*Sobell Department of Motor Neuroscience and Movement Disorders, UCL Institute of Neurology, University College London, London, WC1N 3BG, UK*

DOI: 10.1523/ENEURO.0159-18.2018

Received: 23 April 2018

Accepted: 8 May 2018

Published: 4 June 2018

Author Contributions: K.Y., B.F. and S.B conceived the research programme. C.K., L.S. and K.Y. designed the experiment; C.K. and L.S. conducted the research and analysed the data; C.K. drafted the paper, which all authors critically revised and approved.

Funding: http://doi.org/10.13039/501100000275Leverhulme Trust
RPG-2014188

Conflict of Interest: Authors declare no conflict of interest.

This work was funded by a Leverhulme Trust Research Project Grant (RPG-2014188).

LS and CK are contributed equally to this work.

Correspondence: Carmen Kohl, City University of London, Rhind Building, EC1V 0HB, London. E-mail: carmen.kohl@city.ac.uk

Cite as: eNeuro 2018; 10.1523/ENEURO.0159-18.2018

Neurodynamic Evidence Supports a Forced-Excursion Model of Decision-Making under Speed/Accuracy Instructions

Abbreviated title: Neural signals support forced-excursion SAT model

Laure Spieser [1,2], Carmen Kohl [1,2,], Bettina Forster [2], Sven Bestmann [3], Kielan Yarrow [2]

[1] These authors contributed equally

Author Affiliations:

[2] Department of Psychology, Cognitive Neuroscience Research Unit, City, University of London, EC1V 0HB, UK

[3] Sobell Department of Motor Neuroscience and Movement Disorders, UCL Institute of Neurology, University College London, WC1N 3BG, UK

Author Contributions: K.Y., B.F. and S.B conceived the research programme. C.K., L.S. and K.Y. designed the experiment; C.K. and L.S. conducted the research and analysed the data; C.K. drafted the paper, which all authors critically revised and approved

Correspondence:
Carmen Kohl
City University of London
Rhind Building
EC1V 0HB
London
carmen.kohl@city.ac.uk

Number of figures: 4
Number of Tables: 2
Number of Multimedia: 0
Number of words for Abstract: 243
Number of words for Significance Statement: 114
Number of words for Introduction: 707
Number of words for Discussion: 1996

Conflict of Interest: The authors declare no competing financial interests.
Funding Sources: This work was funded by a Leverhulme Trust Research Project Grant (RPG-2014188).

Abstract

Evolutionary pressures suggest that choices should be optimised to maximise rewards, by appropriately trading speed for accuracy. This speed-accuracy tradeoff (SAT) is commonly explained by variation in just the baseline-to-boundary distance, i.e. excursion, of accumulation-to-bound models of perceptual decision making. However, neural evidence is not consistent with this explanation. A compelling account of speeded choice should explain both overt behaviour and the full range of associated brain signatures. Here, we reconcile seemingly contradictory behavioural and neural findings. In two variants of the same experiment, we triangulated upon the neural underpinnings of the SAT in the human brain using both EEG and TMS. We found that distinct neural signals, namely the ERP centroparietal positivity (CPP) and a smoothed motor-evoked potential (MEP) signal, which have both previously been shown to relate to decision-related accumulation, revealed qualitatively similar average neurodynamic profiles with only subtle differences between SAT conditions. These signals were then modelled from behaviour by either incorporating traditional boundary variation or utilising a forced excursion. These model variants are mathematically equivalent, in terms of their behavioural predictions, hence providing identical fits to correct and erroneous reaction time distributions. However, the forced-excursion version instantiates SAT via a more global change in parameters and implied neural activity, a process conceptually akin to, but mathematically distinct from, urgency. This variant better captured both ERP and MEP neural profiles, suggesting that the SAT may be implemented via neural gain modulation, and reconciling standard modelling approaches with human neural data.

Significance Statement

Successful organisms need to make the right choice fast. To make such decisions, we are regularly forced to trade speed for accuracy. This tradeoff has been explained in behavioural models using a single free parameter reflecting response caution. However, neural evidence suggests that more widespread changes are associated with quick vs accurate decisions. Here, we suggest a model which reconciles these seemingly contradictory findings. This 'forced-excursion' model is mathematically equivalent to standard models of response caution but implies a global modulation in activity akin to a change in neural gain or urgency. Re-expressed in this way, the model is able to account for both behavioural and neural data from two separate neural recording techniques.

Introduction

Every day we make countless decisions, each requiring an appropriate compromise between speed and accuracy. This speed-accuracy tradeoff (SAT, Garrett, 1922; Hick, 1952; Wickelgren, 1977) appears ubiquitous across experimental tasks and species (Chittka et al., 2003; Heitz and Schall, 2012; Ivanoff et al., 2008). The process of making decisions can be formally described using sequential sampling models: Sensory evidence accumulates over time, until a decision boundary is reached, triggering a response (Brown and Heathcote, 2008; Ratcliff, 1978). Such models traditionally explain SAT-related changes in the reaction-time distributions of both correct and erroneous responses by adjusting their boundary parameter. This reduces the required accumulation excursion, leading to faster but more error-prone decisions (Bogacz et al., 2006; Brown and Heathcote, 2008; Smith and Ratcliff, 2004; Usher and McClelland, 2001).

Signals displaying the accumulation predicted by these models have been identified in electrophysiological data from non-human primates (Gold and Shadlen, 2000; Shadlen and Newsome, 1996, 2001), and recently also in humans (Donner et al., 2009; Hadar et al., 2016; O'Connell et al., 2012). However, when instructions or payoffs change, neural accumulation profiles appear inconsistent with a changing boundary, the traditional model-based explanation of the SAT (Hanks et al., 2014; Heitz and Schall, 2012, 2013).

Hanks et al. (2014) proposed that the SAT is explained by an urgency signal in monkeys. Similarly, a recent human neuroimaging study proposed that urgency may arise from a global modulation of neural gain (Murphy et al., 2016). In fact, the

concept of an evidence-independent urgency signal, which increases over time to inflate the accumulation process, has been a recurring theme in the recent SAT literature (Cisek et al., 2009; Milosavljevic et al., 2010; Thura et al., 2012). This urgency signal may increase faster under speed instructions, leading to faster, more error-prone responses. However, alternative accounts, prioritising human behavioural data, favour models which implement boundary differences (hereafter referred to as “classic” models) as opposed to urgency signals (Hawkins et al., 2015; see also Evans et al., 2017).

Here, we aimed to square these contrasting behavioural and neural findings. In classic models, the use of a varying boundary to explain the SAT is in fact merely a conceptually appealing convention. Since sequential sampling models are formally non-identifiable (i.e. different parameter combinations can yield the same prediction), one parameter must be chosen as a scaling parameter and fixed to an arbitrary value (i.e. changing its value will lead to a change in the value of all parameters but not in their relation to each other and therefore will not affect the model fits; Donkin et al., 2009; Ratcliff and Rouder, 1998). This suggests that a variant of the classic model could be used to transfer the effects of the SAT onto other model parameters, while providing an equivalent fit to the data. We hypothesised that this mathematical sleight of hand would reconcile the classic bound-variation explanation of the SAT with neural findings.

We tested this hypothesis against data from two experiments. Experiment 1 used transcranial magnetic stimulation (TMS) to track corticospinal excitability, a downstream signal presumed to be under continuous influence from the decision

variable (Bestmann et al., 2008; Duque et al., 2010; Hadar et al., 2016; Klein-Flugge and Bestmann, 2012). In Experiment 2, we recorded the event-related potential (ERP) centroparietal positivity (CPP; Kelly and O'Connell, 2013; O'Connell et al., 2012; Twomey et al., 2016), a large, late positivity recorded over parietal regions. Importantly, this ERP has been suggested to reflect decision-related accumulation directly, independently of associated motor responses. These ERP and MEP signals therefore represent fundamentally different neural generators, which have both been shown to reflect decision-making processes. We believe that this methodological triangulation permits a more robust interpretation that spans the sensorimotor pipeline.

In both experiments, participants made decisions with two difficulty levels under SAT instructions. Difficulty influences the rate of evidence accumulation (Donkin et al., 2011; Ratcliff and McKoon, 2008), and was introduced here to confirm that our signals represented plausible correlates of the decision variable. We then constructed accumulation profiles predicted when the SAT is modelled through boundary variations, and by our alternative forced-excursion approach. By comparing these neurodynamic predictions to data, we demonstrate that classic models re-expressed to have a fixed excursion provide compelling approximations to both brain and behavioural measures in humans.

Materials & Methods

Participants

For the TMS experiment, an opportunity sample of 22 participants (13 female), primarily students and staff at City, University of London were recruited. According to criteria established prior to the experiment, participants were excluded if they were unable to reach a calibrated coherence level of less than 90% for either of the difficulty conditions (see *Difficulty Calibration*). The remaining 18 participants (11 female, mean age of 29.82, *SD* = 8.38) took part in three sessions, each lasting between 2 and 2.5 hours and involving the same conditions (speed/accuracy easy/hard, see below). For the EEG experiment, we recruited 26 participants (17 females). Of these, 23 (15 females), with a mean age of 29.39 (*SD* = 7.47), pre-tested sufficiently well to proceed to the main experiment, and thus participated in a single 2-hour session. All participants were paid £8 per hour and an additional reward for task performance (up to £4 per session). The experiments were approved by the City, University of London Psychology Department Ethics Committee.

Stimuli and Procedure

< Insert Figure 1 around here >

Stimuli and Experimental setup

In the random dot motion task (Figure 1 a), participants saw an array of moving dots, a proportion of which moved coherently in one direction (equiprobably up or

down) while the rest moved in random directions (selected for each dot on each frame). Trial difficulty was manipulated by varying the proportion of dots moving coherently. The task was displayed on a cathode ray tube (CRT) screen (size: 41 cm x 30 cm), operating at a refresh rate of 85 Hz and a resolution of 1240 x 786 pixels. Participants sat at a distance of 100 cm from the screen. In each trial, 300 white dots, each 0.04 x 0.04 degrees visual angle (dva) in size, were displayed within a 5 dva aperture on a black background. A fixation cross (size: 0.33 x 0.33 dva) was located centrally. All dots moved at a speed of 3.3 dva per second. The position of all dots was randomised every five frames. The experiment was coded in Matlab (The Mathworks, Natick, U.S.A.), using the Psychophysics Toolbox extension (Brainard, 1997; Kleiner et al., 2007; Pelli, 1997) and run on a PC.

Initially, participants saw a fixation cross for 500 ms (plus a jitter of up to 1000 ms, drawn from a uniform distribution). Then, 100% of the dots moved randomly for 1000 ms (plus a jitter of up to 1500 ms, drawn from a truncated gamma distribution with shape parameter 1 and scaling parameter 150). This was followed by the onset of coherent motion, either upwards or downwards, for up to 2000 ms, or until response. Feedback was provided after each trial (see *SAT Instructions*). Two equiprobable coherence levels generated 'easy' (high coherence) and 'hard' (low coherence) trials, which were randomly intermixed. The 'speed' and 'accuracy' conditions were blocked. The order of these SAT blocks was counterbalanced across participants.

Each participant completed a minimum of 100 practice trials, followed by 200 calibration trials (see *Difficulty Calibration*). In each experimental TMS (EEG) session, a total of 432 (800) planned trials were completed, and self-timed breaks

were provided after every 50 (100) trials. In TMS sessions, to ensure the required frequency of pulses (< .2 Hz), TMS-free trials were added when necessary (see *TMS and EMG Processing*), leading to an average of ~500 trials per session.

Responses

Participants in the TMS experiment held two digital response buttons interfaced via a 16 bit A/D card (National Instruments X-series PCIe-6323, sample rate 100,000 Hz) in their right hand. One button was placed between the thumb and index finger and required a 'pinch' response, contracting the first dorsal interosseous (FDI) muscle. The second button was placed on a plastic cylinder in the palm of the hand and required a 'grasp' response, contracting the abductor digiti minimi (ADM) muscle (Figure 1 b). The pinch and grasp buttons indicated 'up' and 'down' responses respectively. In the EEG experiment, participants held one button between the thumb and index finger of each hand, with right and left-hand button presses indicating upward and downward motion respectively.

Difficulty Calibration

Once participants felt comfortable with the task, they completed a total of 200 staircase trials to calibrate the level of difficulty appropriate for the 'easy' and 'hard' conditions. A QUEST procedure (Watson and Pelli, 1983) estimated the coherence levels at which each participant responded correctly in 75% and 95% of trials, used for the 'hard' and 'easy' conditions respectively. The stimulus presentation time was reduced from 2000 ms to 1300 ms, and no feedback was

provided during QUEST trials. If a participant's performance led to estimated hard coherence levels of more than 90%, the participant was excluded from the experiment. This procedure resulted in a mean coherence of 23.81% in the hard condition and 65.41% in easy trials in the TMS experiment, and 30.63% for hard, and 67.67% for easy trials in the EEG experiment.

SAT Instructions

After the difficulty calibration, the main experiment began, in which, participants were instructed to react either as fast or accurately as possible in different blocks. Additionally, feedback was provided after each trial to either reward participants (by display of the word 'Correct' and a small monetary reward, adding up to a maximum of £4 per participant) for fast and correct/correct responses in 'speed'/'accuracy' trials respectively, or provide negative feedback (with the words 'TOO SLOW' or 'INCORRECT' in green letters on a red screen) when the instructions were not followed. The inter-trial interval was increased by 1000 ms after each trial with negative feedback. Neutral feedback (no monetary reward, but a neutral screen with the words 'incorrect' or 'too slow') was shown when participants responded fast but incorrectly in the 'speed' condition or accurately but very slowly in the 'accuracy' condition. Whether a response was too slow or not was determined by a variable deadline which was initially set to 600 ms for the 'speed' and 1000 ms for the 'accuracy' condition. To optimise performance, the deadlines varied between 450 and 750 ms ('speed') and between 700 and 1300 ms ('accuracy') and were adjusted using separate QUEST procedures, targeting accuracy levels of 75% for 'speed',

and 90% for 'accuracy' conditions. Feedback was also provided when participants responded before the onset of the coherent motion ('too fast').

TMS and EMG Processing

In the TMS experiment, participants' muscle activity was recorded using surface electromyography (EMG), sampled at 1000 Hz via a 13 bit A/D Biometrics Datalink system (version 7.5, Biometrics Ltd., Ladysmith, VA, U.S.A., 2008). We placed 22 mm x 28 mm surface Ag/AgCL electrodes on the skin above the FDI and the ADM of the right hand, as they contribute to the 'pinch' and 'grasp' responses respectively. Reference electrodes were placed at distances of approximately 2 cm to each active electrode. Participants were instructed to relax their hand muscles in between responses, and the EMG signals were passed to two speakers to provide auditory feedback about any unwanted muscle activation.

During the experiment, single-pulse TMS was applied using a MagstimRapid^2 biphasic stimulator (Magstim Co. Ltd., Whitland, UK). A figure-of-eight coil was positioned over the optimal spot on the scalp over the left primary motor cortex to elicit MEPs in both the ADM and FDI. The exact location was adjusted for each participant and the stimulation intensity was set at approximately 110% of the resting motor threshold, in order to evoke potentials of around 1 mV in both muscles. The resting motor threshold was defined as the minimal intensity necessary to elicit an MEP with a peak-to-peak amplitude of ~50 μV in 50% of stimulations in both the FDI

and the ADM, and was, on average, 59.28% (*SD* = 7.76) of maximum stimulator output.

TMS pulses were planned in 66% of trials, but cancelled if a response was detected before stimulation. To ensure a good distribution of TMS pulses over the course of the reaction time, TMS trials were divided into four equally sized, equiprobable time bins (between 5 ms and 500 ms relative to the onset of the coherent motion in the 'speed' condition, and between 5 ms and 600 ms in the 'accuracy' condition). Within a given bin, the exact stimulation time was drawn uniform randomly. Since the experiment followed a single-pulse TMS protocol, pulses were required to occur at a maximal frequency of 0.2 Hz. If, by chance, a planned pulse followed a previous one after less than 5000 ms, the task was adjusted in several ways. If the timespan between the previous and the planned pulse was less than 5000 ms but more than 4000 ms, the inter-trial interval was increased in order to decrease the pulse frequency to < 0.2 Hz. For scheduled intervals of less than 4000 ms, the planned trial was replaced with the next planned stimulation-free trial. If no stimulation-free trial remained, random stimulation-free trials were generated in order to increase the interval between TMS pulses, resulting in an average of 68.67 (*SD* = 15.79) additional trials per session.

EMG pre-processing

To eliminate potential differences in the time required to execute 'pinch' and 'grasp' responses, we recorded the onset of EMG as a measure of reaction time (EMG RT). EMG data from both channels were aligned to the onset of the coherent motion

(stimulus onset) and visually inspected to select the onset of response-related EMG bursts. Visual inspection provided no information about the experimental condition of a given trial.

In TMS trials, MEP amplitudes in both channels (FDI and ADM) of the right hand were defined as the difference between the minimal and maximal EMG values in a time window of 10 to 40 ms relative to stimulation time. An algorithm detected EMG activity prior to the stimulation, discarding any trials in which there was activity greater than 50 μV peak to peak in a period of 200 ms preceding the stimulation. These trials, as well as trials in which there was partial activation in more than one channel, or trials in which a clear EMG onset could not be detected, were excluded from further analysis (23.39% of trials). Additionally, trials with very fast (< 100 ms) or very slow (> 1800 ms) response onsets (5.12% of trials), trials in which no MEP was visible or in which the MEP amplitude could not be accurately detected due to amplifier saturation (1.05%), and trials in which the response preceded the planned TMS pulse (6.09%) were excluded. In total, 35.65% of all trials were discarded, with a total of 17,067 trials remaining, including 6535 usable TMS trials (42.85% of all planned TMS trials).

MEP processing

To yield sufficient data to accurately estimate corticospinal excitability in a time-continuous manner, correct-trial MEPs from all participants were combined. Before pooling, MEP amplitudes were z-transformed separately for each muscle, session and participant, while TMS latencies were normalised by median RT of TMS-free

trials in the corresponding session. Z-scored MEPs were then sorted as a function of stimulation latency (Figure 1 c, e, f) and smoothed using a Gaussian kernel to recover a continuous time-varying MEP average in steps of 1% median RT:

$$\hat{Y}(t) = \frac{\sum_{i=1}^{N} e^{\left(-\frac{(t-t_i)^2}{2\sigma^2}\right)} Y_i}{\sum_{i=1}^{N} e^{\left(-\frac{(t-t_i)^2}{2\sigma^2}\right)}} \quad (1)$$

Where the N contributing MEPs each have amplitude Y_i and occur at normalised time t_i. The width of the Gaussian kernel defined by the full width half maximum was set at 5% of median RT (i.e., around 20ms), previously suggested as an appropriate compromise between temporal resolution and signal-to-noise ratio (Hadar et al., 2016). This MEP signal was computed for both stimulus and response-locked MEP latencies, and from the responding muscle, the non-responding muscle and the MEP amplitude difference between them. Finally, 95% confidence intervals were estimated around each signal using a bias-corrected and accelerated bootstrap (BCa) confidence interval, based on 1999 iterations. Since analyses were restricted to correct trials, MEPs recorded from the responding muscle always reflected activation of the correct response, while MEPs form the non-responding muscle reflected the incorrect response. We focused particularly on the MEP average signal based on the amplitude difference between responding and non-responding MEPs, as this eliminates variations due to non-specific influences, such as inhibitory processes during action preparation, which would result in MEP suppression in both responding and non-responding muscles (for a review see Duque et al., 2017).

EEG Recording and Processing

Continuous EEG was recorded using 64 active electrodes, placed equidistantly on the scalp (EasyCap, M10 Montage) and referenced to the right mastoid (BrainAmp amplifier; BrainProducts; sampling rate: 1000 Hz). The data were pre-processed and analysed using custom scripts in Matlab (Mathworks, Natick, USA), drawing on functions from the EEGLAB toolbox (Delorme and Makeig, 2004).

EEG data were re-referenced to the average reference and digitally bandpass filtered (0.1 to 45 Hz). Data were visually inspected to remove large muscle artefacts before applying ICA to remove eye blink components. Any remaining artefacts were removed manually during a second visual inspection. Afterwards, spherical spline interpolation was used to reconstruct noisy channels, which were identified and rejected during the first visual inspection. In line with the procedures used in previous CPP studies (Kelly and O'Connell, 2013; O'Connell et al., 2012), the data were converted to current source density (CSD) estimates using the CSD toolbox (Kayser and Tenke, 2006).

Experimental Design and Statistical Analysis

Behavioural Data Analysis

We explored the within-subjects factors Instruction and Difficulty with the levels speed/accuracy and easy/hard respectively. To test their effects on RT, we used a 2x2 repeated-measures ANOVA. Because accuracy data violate the assumptions of ANOVA, statistical inferences about errors were made using a generalised linear

356 mixed-effects model with a logistic link function and binomial data model (applied
357 using the 'fitglme' function in Matlab). Parameter estimates were based on a
358 maximum-likelihood method using Laplace approximation and the 'maximal' random
359 effects structure (Barr et al., 2014), i.e. both Instruction and Difficulty, and the
360 Instruction*Difficulty interaction were entered as fixed effects, and both
361 manipulations, and their interaction within each participant (and session in the TMS
362 experiment) were included as random effects.

363

364 **MEP Analysis**

365 Two analyses were conducted on the MEP difference signal to confirm that MEP
366 modulations across time reflected decision-related accumulation processes. We
367 compared the stimulus-locked build-up rate, expected to be steeper in easy than
368 hard trials, and the response-locked signal amplitude, which should not vary across
369 difficulty levels at the time of decision. Comparisons were also made across speed
370 instructions, although no clear predictions could be made regarding how evidence
371 accumulation should vary in this case. MEP data were permuted across easy and
372 hard (or across speed and accuracy) trials1999 times. Mean MEP signals (and 90%
373 BCa confidence intervals; see below) were then computed for each iteration. The
374 build-up rate was then estimated from both the original and the resampled data as
375 the slope of a straight line fitted to the stimulus-locked signal in a time window
376 ranging from half median up to median RT (corresponding to around 200 to 400 ms
377 after stimulus onset). Slope differences between difficulty levels or instructions were
378 considered significant if smaller (or larger) than the lower (or upper) 2.5% of the
379 corresponding slope-difference null distribution obtained from resampled signals.

To test response-locked amplitude differences while controlling for multiple comparisons, a cluster statistic was calculated (c.f. Blair and Karniski, 1993; Groppe et al., 2011; Nichols and Holmes, 2001). Potential regions of difference between conditions were based on contiguous time periods with no overlap between 90% bootstrap BCa confidence intervals (the arbitrary "cluster threshold"). A cluster sum was calculated within each such putative cluster, and was considered significant when this sum of the point-by-point differences fell outside the central 95% of the corresponding distribution of the biggest cluster sum obtained from resampled signals. Amplitude differences were assessed on both stimulus and response-locked signals.

ERP Analysis

For the ERP analysis, we extracted both stimulus (-200 to 2000 ms, relative to coherent motion onset) and response aligned (-1000 to 100 ms, relative to the button press) epochs. All epochs were baseline corrected to the average over a 200 ms period preceding motion onset. The appropriate electrode to generate the CPP waveform was chosen individually, by visually inspecting each participant's averaged ERP topography to identify the centroparietal region of maximum amplitude (chosen electrodes: 1, 5, or 14, roughly equivalent to electrodes Cz, CPz, Pz in the 10-20 system). The activity recorded on the selected electrode was averaged for each condition (collapsed over 'up' and 'down' trials) and for stimulus and response-locked signals separately. In line with Kelly and O'Connell (2013), we measured the slope of the CPP for each participant, by fitting a straight line to the waveform from 200 to

350 ms in the stimulus-locked data. Additionally, we measured the peak amplitude of the response-locked ERP by averaging over the amplitude of the waveform from -50 to 50 ms relative to the response. Differences across conditions were assessed with a 2x2 repeated-measures ANOVA.

Modelling

Free-excursion race model

According to a standard free-excursion race model (Bogacz et al., 2006; Laberge, 1962; Vickers, 1970) evidence supporting the correct and the incorrect response is integrated independently in two accumulators. The amount accumulated at each time step (dx) is given by:

$$\mathrm{d}x_{\mathrm{correct}} \propto v_{\mathrm{correct}} + N(0,\sigma^2)$$
$$\mathrm{d}x_{\mathrm{incorrect}} \propto v_{\mathrm{incorrect}} + N(0,\sigma^2) \quad (2)$$

Where x_{correct} and $x_{\mathrm{incorrect}}$ are the quantities accumulated, and v_{correct} and $v_{\mathrm{incorrect}}$ the input evidence (i.e. accumulation rate, see below) in favour of the correct and the incorrect responses. Noise, N, drawn from a normal distribution of mean 0 and standard deviation σ, is also integrated at each iteration. To avoid negative values, evidence accumulated at each time step is updated as:

$$x_{\mathrm{correct}}(t+1) = \max(0,\ x_{\mathrm{correct}}(t) + \mathrm{d}x_{\mathrm{correct}})$$
$$x_{\mathrm{incorrect}}(t+1) = \max(0,\ x_{\mathrm{incorrect}}(t) + \mathrm{d}x_{\mathrm{incorrect}}) \quad (3)$$

Correct and incorrect accumulator starting points are drawn in each trial from a uniform distribution ranging between 0 and S_Z. As soon as one of the accumulators reaches the response boundary A, the corresponding response is selected. The response time is then modelled as the time required to reach the boundary, plus non-decision time, during which sensory and motor processes occur, drawn from a uniform distribution centred on T_{er} and of width S_{Ter}. In a standard race model for a binary decision, this leads to a total of seven parameters (A, S_z, $v_{correct}$, $v_{incorrect}$, T_{er}, S_{Ter}, σ^2). One parameter is chosen as a scaling parameter and fixed to an arbitrary value, resulting in a total of six free parameters.

To apply this model to the data in this experiment, we added accumulation rate parameters to account for the different difficulty conditions ($v_{easy\_correct}$, $v_{easy\_incorrect}$, $v_{hard\_correct}$, $v_{hard\_incorrect}$). This implementation of difficulty is well-established and has been validated using both behavioural and neural data (Mulder et al., 2014; Ratcliff and McKoon, 2008; Ratcliff and Rouder, 1998; Roitman and Shadlen, 2002; Twomey et al., 2015). In order to explain differences due to SAT instructions, we added a second boundary parameter. The boundary for 'accuracy' trials $A_{accuracy}$ acted as a scaling parameter and was fixed to 1, while the boundary for the 'speed' condition, A_{speed}, was free to vary. We tested three different models: one in which all remaining parameters were fixed across conditions (Model 1), one in which the starting point parameter S_z was free to vary across SAT conditions (Model 2), and one in which the non-decision time parameter T_{er} was free to vary across SAT conditions (Model 3; see Table 1).

Modelled RTs were simulated based on Equations 2 and 3 (10,000 simulated trials with a 1% median RT time step, around 4ms, for TMS and a 10ms time step for EEG) and compared to pooled RT data using Quantile Maximum Probability Estimation (Heathcote et al., 2002). Specifically, we estimated empirical RT quantiles (at 0.1, 0.3, 0.5, 0.7 and 0.9), for both correct and erroneous responses, and compared counts of simulated RTs in the resulting bins against the predicted multinomial distribution. Parameter values were adjusted using a differential evolution algorithm implemented in Matlab (Price et al., 2005). The goodness-of-fit of the different models was assessed by computing the Akaike information criterion (AIC, Akaike, 1977).

Forced-excursion Race model variant

To test the hypothesis that the SAT is not implemented through decision bound variation *per se*, but rather by more widespread changes of neural activity, we constructed a forced-excursion model variant in which decision boundaries are fixed and the effects of the SAT are transferred onto all other parameters. All parameters of the free-excursion race model estimated in the speed condition were divided by the speed boundary A_{speed} (apart from T_{er} and S_{Ter}). This forced-excursion version of the model is mathematically equivalent to the original one as, given the scaling property of sequential sampling models, multiplying all models parameters (except T_{er} and S_{Ter}) by the same amount does not affect model predictions (Donkin, Brown, et al., 2009). A simple 'rescaling' of speed parameters hence results in a new set of parameters in which the speed and accuracy response boundaries are equal, and the SAT modulation is transferred onto the other decision-related parameters.

475

476 **Model predictions**

477 *TMS experiment:* In each session, EMG RTs were normalized by median EMG RT,
478 and trials were pooled across sessions and participants. On average, we obtained
479 2,651 trials per condition, used to determine best-fitting parameters at the group
480 level. We then generated predictions according to the free and forced-excursion race
481 model variants by simulating evidence accumulation. To allow for a direct
482 comparison, model predictions were constructed identically to the accumulation
483 signals derived from our experimental data, i.e., as MEP difference average signals.

484

485 For both models, and each condition, 20,000 single-trial accumulation paths were
486 computed based on Equations 2 and 3 (in 0.5% median EMG RT time steps). Each
487 modelled MEP amplitude was determined by the value of one of the single-trial
488 simulated accumulation signals reached at a (simulated) TMS latency, based on
489 stimulation times applied during the experiment (see Figure 1 d-f). The difference
490 between correct and incorrect values was used to model the MEP difference signal.
491 As in experimental data, trials were discarded when simulated RT was shorter than
492 TMS latency (i.e., the response would have been given before the TMS pulse). The
493 duration of sensory and motor processes, which are represented by a single T_{er}
494 parameter, have to be allocated to pre and post-accumulation processes in order to
495 generate predictions. Since we modelled accumulation observed in or around M1,
496 we assumed that post-accumulation stages would only relate to response execution,
497 which could reasonably be ignored, as reaction times were defined up to EMG onset.

Therefore, the whole of T_{er} was allocated to pre-accumulation processes, and accumulation started after a delay of $T_{er} \pm S_{Ter}$.

From simulated MEPs, predicted continuous MEP signals were then computed by applying the same smoothing method applied to the MEP data. Finally, accumulation signals based on predicted MEPs were compared to the empirical MEP signal using a mean squared error metric, after a scaling procedure was applied to match modelled and experimental signal amplitudes. Modelled signals were vertically normalized by the value minimizing the mean squared error, estimated using the previously described differential evolution algorithm. Note that even though this normalization could differ between the free and forced-excursion models, the same value was applied within each model to all conditions, and to stimulus and response-locked signals.

Finally, two complementary statistical analyses compared the mean squared errors obtained for the free and forced-excursion model variants, to determine which predictions displayed greater similarities to the neural signal. First, goodness-of-fit of the model predictions was computed based on AIC values, using the formula AIC = n*log(MSE) + 2K (Burnham and Anderson, 2004), where n is the number of observations, MSE the mean squared error, and K the number of free parameters (K=1 in this case, as only amplitude was allowed to vary freely to fit recorded MEP signals). AIC was then used to compute Akaike *model weights*, which can be seen as the weight of evidence in favour of each model.

The second analysis applied a bootstrap procedure estimating the distribution of differences of mean squared error between the free and forced-excursion models, in order to determine the bias-corrected[1] 95% confidence interval around the observed difference. To estimate the distribution, EMG RT data were resampled 1999 times with replacement within each condition. The best-fitting parameters for the original and each resampled set of EMG RT data were then estimated by a simplex algorithm implemented in Matlab (Lagarias et al., 1998), using the original parameters as starting values[2]. As for the original analysis, forced-excursion parameters were obtained by normalising the free-excursion parameters by the response boundary value obtained in the speed condition, and MEP signal predictions for free and forced-excursion models were computed. Mean squared errors were then calculated between these bootstrapped signal predictions and a set of equivalently resampled MEP signals, again after applying a scaling procedure matching signals amplitudes (via a differential evolution algorithm, Price et al., 2005). The 95% bias-corrected confidence interval was estimated based on the bootstrap distribution of mean squared error differences between the free and forced-excursion models.

EEG experiment: RTs were pooled across participants to fit the models at a group level. As EEG signals integrate spatially disparate underlying neuronal activity, we reasoned that the CPP would likely represent the sum of evidence accumulators across time. The corresponding accumulation signals predicted by the models should therefore be obtained by adding up the correct and incorrect accumulators'

[1] Bias-correction was used rather than bias-correction and acceleration (BCa) to make the time of computation manageable.
[2] The Simplex algorithm was preferred to the differential evolution algorithm in this case to reduce the time of computation.

545 activities. For both models and each speed and coherence level condition, 10,000
546 single-trial accumulation paths were computed based on Equations 2 and 3. To
547 account for sensory processes, accumulation started after a sensory delay. Once a
548 decision was made, we assumed that evidence accumulation continued until the
549 response was executed (and the stimulus was turned off). Accumulation therefore
550 continued after the boundary was reached for the duration of any motor processes
551 (Resulaj et al., 2009; Twomey et al., 2015). The compound duration of sensory and
552 motor processes were given by the model non-decision time T_{er}, which we divided
553 into T_e and T_r, modelling sensory and motor processes respectively. As detailed
554 below, this division was optimized for each model. To match with EEG processing,
555 the sum-of-accumulations signal was baseline corrected by subtracting the first data
556 point value from each trial. Finally, to compare the prediction to the CPP, we
557 averaged accumulation signals in each condition, either time-locked on stimulus
558 onset (i.e., time 0), or on response time (the time of the corresponding simulated
559 RT). Since we can only speculate on how the accumulator behaves once the
560 response is executed, trials were removed from averaging once the simulated
561 response time had been reached (and the same procedure was used for the
562 averaging of empirical EEG data).
563
564 The similarity between the CPP and the predicted decision variable of each model
565 was quantified by computing the mean squared error between mean signals. To
566 provide optimal CPP predictions, the amplitude of each summed signal was scaled
567 to match the CPP amplitude, and the division of non-decision time T_{er} into encoding
568 time T_e and response time T_r was determined. The optimal scaling factor and T_{er}

569 division were obtained for each model signal using differential evolution (Price et al.,
570 2005), minimising the mean squared error.
571
572 Finally, as in the TMS experiment, a bootstrap analysis (bootstrapping both RT and
573 EEG data) determined whether the mean squared error calculated for the free- and
574 the forced-excursion models had a 95% confidence interval excluding zero, i.e.
575 whether they differed significantly. In this experiment, no AIC-based comparison was
576 attempted because EEG data points have complex temporal dependencies (i.e.
577 autocorrelation) that make it difficult to establish the likelihood with which a model
578 predicts these neurodynamic data.
579

580 Results

581 Behavioural Results

582 Trials remaining after pre-processing were collapsed over 'up' and 'down' trials
583 (Figure 2). Both experiments revealed the same behavioural effects. As expected,
584 RTs were faster under speed than accuracy instructions (TMS: $F(1,17) = 26.90$, $p <$
585 .001, $\eta_p^2 = .61$; EEG: $F(1,22) = 36.47$, $p < .001$, $\eta_p^2 = 0.62$), as well as in easy
586 compared to hard trials (TMS: $F(1,17) = 62.14$, $p < .001$, $\eta_p^2 = .79$; EEG: $F(1,22) =$
587 120.12, $p < .001$, $\eta_p^2 = 0.85$). Additionally, Instruction and Difficulty interacted (TMS:
588 $F(1,17) = 10.80$, $p = .004$, $\eta_p^2 = .79$; EEG: $F(1, 22) = 36.47$, $p < .001$, $\eta_p^2 = .62$).
589 Follow-up t-tests revealed that the effect of difficulty was larger in the accuracy
590 condition ($p < .001$) than in the speed condition ($p < .001$). All reported effects in the

591 TMS experiment are based on EMG RT (time of EMG onset), but results based on
592 response-button RT were not qualitatively different.
593
594 For error data, a generalised linear mixed-effects model revealed higher accuracy
595 scores under accuracy compared to speed instruction (TMS: $t(208) = 4.81$, $p < .001$;
596 EEG: $t(88) = 7.76$, $p < .001$), as well as in easy trials compared to hard trials (TMS:
597 $t(208) = 4.57$, $p < .001$; EEG: $t(88) = 4.68$, $p < .001$). The Instruction*Difficulty
598 interaction was not significant ($p > .05$).
599
600 < Insert Figure 2 around here >

601 ## Neural Results

602 ### MEP-average signals

603 MEP amplitudes from correct trials were collated and smoothed to form three
604 categories of MEP-average signal: Responding, non-responding, and the difference
605 between them. Responding and non-responding MEP-average signals obtained for
606 each condition are presented in Figure 3 a. The responding MEP-average signal
607 (associated with the correct response) builds up gradually during the reaction time
608 period, while the non-responding signal (associated with the incorrect response)
609 remains fairly flat. However, our main focus was the difference in MEP amplitudes
610 between responding and non-responding muscles (Figure 3 c). Statistical analyses
611 confirmed that this MEP signal displays characteristics consistent with the
612 hypothesis that M1 excitability reflects an accumulation process. We found that the
613 stimulus-locked signal built up faster in easy than hard trials (for both speed, p =

614 .049, and accuracy, $p < .001$ instructions), and that the response-locked signal
615 amplitude reached similar levels just before the response regardless of trial difficulty,
616 with cluster permutation tests showing no significant divergence between conditions
617 ($p = 1$). Differences were however observed in stimulus-locked averages, with higher
618 amplitudes evident in easy compared to hard trials from 75% median EMG RT (~294
619 ms) in the speed condition (p = .005) and from 81% (~318 ms) under accuracy
620 instructions ($p < .001$). The latter results demonstrate that we had sufficient power to
621 detect MEP amplitude differences. Collectively, our results show that the MEP-
622 average difference signal is a viable neural correlate of the decision variable.
623 However, no difference was observed between speed and accuracy instructions, on
624 either the slope or amplitude of MEP accumulation (all $p > .1$).

625

626 **ERP Results**

627 The CPP is displayed in Figure 3 b. Like the MEP-average difference signal, it builds
628 over the course of the decision, at a rate reflecting the difficulty of the decision. For
629 build-up rate, there was a significant main effect of Difficulty ($F(1,22) = 14.70$, $p =$
630 .001, $\eta_p^2 = .40$), with higher slopes in easy compared to hard trials. There was no
631 main effect for Instruction, and no interaction, in either of the time alignments ($p >$
632 .26).

633

634 There was also a main effect of Difficulty on the peak amplitude of the response-
635 locked CPP, $F(1,22) = 8.53$, $p = .008$, $\eta_p^2 = .28$, with higher amplitudes in the easy
636 compared to the hard conditions. However, again we found no main effect for SAT
637 Instruction and no interaction ($p > .22$).

Summarising the neural data, neurodynamic signals derived from two very different imaging methods converged to yield the same outcome: Clear effects of adjusting task difficulty, particularly on the rate of accumulation, but no statistically reliable effects of speed/accuracy instruction, despite the fact that these two manipulations had similar magnitudes of behavioural effect (mean RT effect sizes, i.e. η_p^2, of 0.62 for SAT instruction vs 0.82 for difficulty).

< Insert Figure 3 around here >

Model selection

In both experiments, we fitted several models to RT data and used AIC to select the best candidate with which to go on and make neural predictions. The winning race model (Model 2; see Table 1) varied both response boundary and starting-point between different SAT instructions (and also varied drift rates with changes in difficulty). As anticipated, the best-supported model's best-fitting parameters (shown under "free-excursion" in Table 2) show that the response boundary decreased under speed instruction, and that accumulation rates were higher for easy than hard trials. Additionally, starting-point variability was larger under speed instructions. Since the starting-point distribution ranges from 0 to the starting-point parameter S_z, larger starting-point variability also implies a larger mean starting-point, further decreasing the distance between baseline and boundary. The quality of the fit was good (see Figure 4).

< Insert Figure 4 around here >

< Insert Table 1 around here >

< Insert Table 2 around here >

Importantly, we also re-expressed this model under a forced-excursion constraint. In this forced-excursion version, parameter normalisation forced the speed response boundary to be the same as the accuracy boundary, with the SAT being transferred onto accumulation rate and variability parameters. Note that the forced-excursion version of this model is mathematically equivalent to the standard one, with identical predicted RTs and error rates.

Stimulus and response-locked accumulation signals for each experiment and each condition predicted by the free and forced-excursion variants of the best-supported model are shown in the lower panels of Figure 3. Broadly the same patterns were predicted in both experiments. The main difference between free and forced-excursion predictions is the level of accumulation reached at the time of the decision. This is evident in the amplitude of response-locked signals attained just before response selection, which is predicted to be higher under accuracy than speed instructions for the free-excursion model, but similar in the forced-excursion model (Figure 3 panels d-h). Note that, while this pattern is more pronounced in the forced-excursion predictions associated with the MEP signal (Figure 3 e) than the EEG signals (Figure 3 h), the reduced amplitude difference between speed and accuracy profiles prior to the response is evident in both experiments, and importantly, both forced-excursion model predictions capture the patterns seen in the corresponding neural data (Figure 3 c, f). In the stimulus-locked predictions, easy trials display a

steeper build-up than hard trials, yet, interestingly, even though accumulation rates in the forced-excursion model were higher under speed than accuracy instructions (see Table 2), the predicted signal was not correspondingly steeper in this case (see Figure 3 panels e, h). For MEPs, this may be partly explained by the fact that both correct and incorrect accumulation rates increased, such that the slope of the (motoric, thus difference-based) accumulation signal remained unaffected. However, the similar pattern observed in CPP predictions (which were modelled as a sum of accumulators, because this signal occurs relatively early and is not response-specific) indicates that the ~20% change in modelled accumulation rate was insufficient to generate a substantial increase in predicted slope when combined with the associated changes in noise parameters.

Summarising these observations, the signals predicted by the forced-excursion version of the best-supported model appear to better reproduce the pattern of the recorded CPP and MEP signals than do those predicted by the free-excursion version. Specifically, the accumulation slope is steeper in easy than hard trials, but not different between speed and accuracy conditions, and a similar signal amplitude is attained before response for both coherence levels, and, crucially, under both SAT instructions.

Statistical analyses confirmed these observations. Akaike weights in the TMS experiment indicated that neurodynamic predictions from the forced-excursion model variant were better matched to the MEP signals than were free-excursion predictions (forced-excursion: 0.994, free-excursion: 0.006). Additionally, bootstrap analysis showed that the mean squared error between predicted MEP signals and recorded

712 MEP values was significantly lower for the fixed than the free-excursion model (p =
713 .018, 95% bias-corrected confidence interval on difference: [0.005; 0.056][3]). The
714 same bootstrap analysis revealed similar results in the EEG experiment, where the
715 forced-excursion model predicted profiles more similar to the CPP than the free-
716 excursion model (p = .026, 95% bias-corrected confidence interval on this difference:
717 [1.55; 21.32])[4].
718
719
720

[3] Although a significant difference was observed using a BCa confidence interval, this was not the case when a simpler percentile interval was used. This result should hence be interpreted cautiously (but is bolstered by our subsequent findings with EEG).
[4] For consistency, we repeated the model comparison for the ERP data set with RT normalised data and found that the results were unchanged.

Discussion

We utilised two separate electrophysiological methods to explore the neurocognitive mechanisms underlying the speed-accuracy tradeoff, a central yet unresolved issue in decision-making research. The model-based behavioural literature suggests that a variation in the decision boundary (or, equivalently, a change in the baseline level) explains the SAT (Brown and Heathcote, 2008; Smith and Ratcliff, 2004; Usher and McClelland, 2001), but recent neural evidence has not supported this claim, suggesting more widespread changes (Hanks et al., 2014; Heitz and Schall, 2012, 2013; Murphy et al., 2016). To resolve this paradox, we hypothesised that the SAT may result from changes which are mathematically equivalent to a modulation of the decision boundary, but which are implemented physiologically through global changes in neural activity akin to turning up the gain in the brain. We recorded neurodynamic substrates of decision-making during a motion discrimination task with two difficulty levels and under instructions to focus on either response speed or accuracy. The resulting data converged to favour the predictions made by a forced-excursion model variant in which the SAT is implemented by adjusting both the signal (i.e. accumulation rates v) and noise (i.e. noise parameters S_z and σ) affecting accumulation-related neural activity.

Although our main interest was the SAT, we included a difficulty manipulation as a "sanity test" regarding the validity of our neurodynamic decision correlates. The impact of difficulty on evidence accumulation has been demonstrated previously, with both sequential sampling models and proposed neural correlates of accumulation displaying steeper build-up rates in easier decisions (Kelly and O'Connell, 2013; Mulder et al., 2014; Ratcliff and McKoon, 2008; Roitman and

745 Shadlen, 2002). Accordingly, we found that faster and more accurate responses in
746 easy trials were explained by higher accumulation rates in both experiments. These
747 patterns were observed in both neural signals and their simulated accumulation
748 profiles and, consistently with previous studies (Hadar et al., 2016; O'Connell et al.,
749 2012), support the role of MEP and CPP signals as neural correlates of the decision
750 variable, with corticospinal excitability likely receiving a time-lagged but continuous
751 input from CPP/decision-generating regions.

752 Like the difficulty manipulation, SAT instructions also resulted in the expected
753 behavioural changes, with faster and more error prone responses under speed
754 instructions. In line with many previous studies (Brown and Heathcote, 2008; Heitz,
755 2014; Ratcliff and McKoon, 2008; Usher and McClelland, 2001), our free-excursion
756 race model accounted for behavioural effects of the SAT, primarily by varying the
757 amount of accumulated evidence required to make a decision. However, since
758 recent studies exploring neural correlates of decision-making have challenged this
759 implementation of the SAT (Hanks et al., 2014; Heitz and Schall, 2012, 2013;
760 Murphy et al., 2016), we used a forced-excursion variant which models a global gain
761 modulation by adjusting the parameters of the free-excursion race model so that the
762 boundary was equal across SAT conditions, thus transferring the estimated
763 difference between response bounds onto all other parameters affecting
764 accumulation. In other words, a fixed boundary between SAT conditions was made
765 mathematically equivalent to the free-excursion model by assuming different
766 underlying mechanisms, with changes between SAT conditions explained not by
767 boundary differences, but by differences between virtually all other parameters,
768 modelling a global shift in decision-related brain activity.

When we compared predicted accumulation profiles from both the free and the forced-excursion model variants to our neural data, a fixed boundary provided significantly better degrees of correspondence between them (we avoid the term "goodness of fit" here, because predictions were based on RT data, with little adjustment required to capture neurodynamic trends). We should, however, offer the caveat that the statistical basis of this result is unconventional. By utilising permutation tests on pooled data, we compared against sampling distributions derived from the population of all possible trials from our particular set of participants, rather than the population of all possible participants. However, generalisations to an even less representative population (e.g. all neurons of a given type within a single monkey) are commonplace in neuroscience. Furthermore, there are several additional observations that support our conclusion that the forced-excursion model variant was best. In both model and data, the stimulus-locked profiles displayed a slope difference between easy and hard trials and no difference between speed and accuracy trials. Importantly, in the response-locked model predictions, the terminal amplitude differences between SAT conditions were reduced compared to the predictions retaining a free excursion, better resembling the neural signals. These findings support the hypothesis that differences induced by SAT instructions are explained by a global modulation of activity rather than by varying a single specific parameter/process.

Previous attempts to explain the SAT in the absence of variation in the decision boundary have done so by incorporating an urgency signal, i.e. an evidence-independent signal, which over time pushes the accumulation process towards a boundary (Cisek et al., 2009; Hawkins et al., 2015; Thura et al., 2012). This integration of urgency is not dissimilar to our suggestion of an amplified

accumulation process. Both approaches avoid a variation in response boundary by boosting accumulation in hasty decisions, and make broadly analogous predictions regarding the SAT's impact on accumulation profiles.

However, urgency models do differ mathematically from our forced-excursion model. While the former assume the addition of an independent and *growing* signal, i.e. a *time-varying* process, the latter is obtained by an adjustment of parameters derived from the more established free-excursion model, implying a *time-invariant* intrinsic amplification of the accumulation process induced by global changes of the system. To expand on this distinction (with the important caveat that the urgency has been implemented in different ways by different authors) – urgency may be implemented as the addition of an evidence-independent signal at each time step*,* with this signal growing over time (e.g. Hanks et al., 2014), or as the multiplication of evidence by such a signal (e.g. Ditterich, 2006) in which case accumulation noise is also subject to this time-varying gain. In the latter approach, the integration of evidence over time may additionally be deliberately downplayed via (very) leaky integration (e.g. Cisek et al., 2009). By contrast, our modelling instead captured the SAT by amplifying both signal and noise in a constant manner *throughout the decision* (with noise even amplified prior to the onset of the imperative stimulus, via the S_z parameter). This is what we mean here by neural gain modulation – the amplification of both signal and noise in a time-independent manner. Note that the way starting-point noise was implemented here implies that it effectively conflates mean starting point with start-point variability (see methods/results). In this sense, our "fixed-excursion" terminology is a slight misnomer – some part of our model's ability to explain the SAT in both behavioural and neural data is still dependent on a reduction in

818 excursion, but several other parameters also play a role, and the decision bound is
819 fixed.

820 We wish to note that we are in no sense hostile to the concept of urgency. In fact, we
821 tested urgency models as an additional exploratory analysis, but opted not to include
822 these results for reasons of brevity and clarity.[5] Indeed, we find the concept of
823 "urgency" to be a useful one that somewhat overlaps our "neural gain" hypothesis
824 and finds support in the neuroscientific literature (e.g. Thura and Cisek, 2017).
825 Therefore, we do not claim that our model is better supported than urgency models,
826 either here or in general. However, since a number of studies evaluating the concept
827 of an urgency signal have been unable to support it, suggesting instead that
828 standard sequential sampling models can fully account for all behavioural data (Balci
829 et al., 2011; Hawkins et al., 2015; Karsilar et al., 2014), we propose that forced-
830 excursion model variants should at least be considered as an appropriate alternative
831 to urgency signals, reconciling decades of model-based support for decision
832 boundary variation with recent neural evidence.

833 Although we have argued that the simulated accumulation profiles of the forced-
834 excursion model closely resemble both of our neural signals, supporting the notion of
835 a global modulation of activity as the underlying mechanism explaining the SAT,
836 there are nonetheless some differences between the empirical and simulated
837 profiles. However, any model is a simplified approximation of the true neurocognitive
838 mechanisms and is unlikely to perfectly simulate any given process. This is
839 particularly the case for neural signals which inherently have a low signal-to-noise-

[5] We implemented two kinds of urgency model, with a linear urgency signal proving more successful. This model was about as good as those we present here when fitting our behavioural data (it provided a better fit in the EEG experiment, but a worse one in the TMS experiment). For neurodynamic data, it performed very similarly to our forced-excursion model in the EEG experiment. Its ability to capture these data in the TMS experiment lay approximately mid-way between our forced and free-excursion classic models, but did not differ significantly from either one.

ratio, such as ERPs and in particular the MEP signal. Somewhat limited signal quality is however typical for experiments of this nature (Hadar et al., 2016; O'Connell et al., 2012), and we used large numbers of trials in both experiments, producing demonstrably interpretable neural signals. We would argue that the correspondence between model predictions and neural data, both here and elsewhere, is remarkable, given a class of models originally conceived to have a largely behavioural scope (Luce, 1986).

All neuroscientific methods have limitations. For example, our MEP signal is derived from a technique that both records and perturbs neural activity, with implications that are difficult to precisely predict (Hadar et al., 2016). However, methodological triangulation is an established approach to building a convincing body of evidence. Here, we obtained converging evidence from two fundamentally different signals, as both corticospinal excitability and a parietal ERP displayed qualitatively similar findings. While there were small practical differences between the experiments (e.g. one vs. multiple sessions, bilateral vs. unilateral responses), these are unlikely to qualitatively alter the accumulation process, and we have matched the simulation of model predictions to the processing of each neural signal to further reduce the impact of methodological differences on our interpretation. Although the suggestion that these signals represent decision accumulation is recent, both signals were modulated by the difficulty manipulation, supporting this account. Furthermore, previous research using more established neural correlates of decision-making in non-human primates has shown similar findings, suggesting widespread changes in activity when the SAT is manipulated (Hanks et al., 2014; Heitz and Schall, 2012, 2013). Collectively, we believe these neural findings warrant adjusting even a well-

established model (by rescaling its parameters) given that the adjustment is purely conceptual and does not affect the behavioural fit.

A final potential concern relates to our decision to fit models to pooled data, i.e. at the group, rather than individual, level. Such collation may give rise to distorted RT distributions relative to the shape of underlying individual distributions. However, where comparisons have been made between the mean of sequential sampling model parameters derived from individual fits, and the same parameters derived from a single group fit, they have tended to suggest that the group fitting approach is not particularly problematic (e.g. Ratcliff et al., 2003, 2004). The procedure has been used in several recent papers (e.g. Dmochowski and Norcia, 2015; Twomey et al., 2015).

In conclusion, we set out to explore the neural mechanisms of the SAT by examining two neural correlates of the decision variable, an MEP signal reflecting corticospinal excitability and a parietal ERP component known as the CPP. The SAT is typically explained in sequential sampling models as a variation of the decision boundary. Here, we tested whether this variation is visible in neural activity or if it might instead be implemented through a mathematically equivalent gain change in neural activity. Our decision-related neural activity, independently sourced from two brain networks, resembled the accumulation profiles predicted by a forced-excursion model variant in which the boundary differences are transferred onto other decision parameters. Consistent with previous studies, our results therefore indicate that the SAT is implemented by global changes of neural activity, but that this conceptually important outcome does not necessarily invalidate traditional modelling approaches.

References

Akaike H (1977) On entropy maximization principle. In: Applications of Statistics (Krishnaiah PR, ed), pp27–41). Amsterdam.

Balci F, Freestone D, Simen P, deSouza L, Cohen JD, Holmes P (2011) Optimal Temporal Risk Assessment. Front Integr Neurosci 5:1–15. http://doi.org/10.3389/fnint.2011.00056

Barr DJ, Levy R, Scheepers C, Tily HJ (2014) Random effects structure for confirmatory hypothesis testing: Keep it maximal. J Mem Lang 68:1–43. http://doi.org/10.1016/j.jml.2012.11.001

Bestmann S, Harrison LM, Blankenburg F, Mars RB, Haggard P, Friston KJ, Rothwell JC (2008) Influence of Uncertainty and Surprise on Human Corticospinal Excitability during Preparation for Action. Curr Biol 18:775–780. http://doi.org/10.1016/j.cub.2008.04.051

Blair RC, Karniski W (1993) An alternative method for significance testing of waveform difference potentials. Psychophysiology 30:518–524.

Bogacz R, Brown E, Moehlis J, Holmes P, Cohen JD (2006) The physics of optimal decision making: A formal analysis of models of performance in two-alternative forced-choice tasks. Psychol Rev 113:700–765. http://doi.org/10.1037/0033-295X.113.4.700

Brainard DH (1997) The Psychophysics Toolbox. Spatial Vision 10:433–436. http://doi.org/10.1163/156856897X00357

909 Brown SD, Heathcote A (2008) The simplest complete model of choice response
910 time: Linear ballistic accumulation. Cognitive Psychol 57:153–178.
911 http://doi.org/10.1016/j.cogpsych.2007.12.002

912 Burnham KP, Anderson DR (2004) Multimodel Inference Understanding AIC and BIC
913 in Model Selection. Sociol Method Res 33:261–304.
914 http://doi.org/10.1177/0049124104268644

915 Chittka L, Dyer AG, Bock F, Dornhaus A (2003) Psychophysics: Bees trade off
916 foraging speed for accuracy. Nature 424:388–388.
917 http://doi.org/10.1038/424388a

918 Cisek P, Puskas GA, El-Murr S (2009) Decisions in Changing Conditions: The
919 Urgency-Gating Model. J Neurosci 29:11560–11571.
920 http://doi.org/10.1523/JNEUROSCI.1844-09.2009

921 Delorme A, Makeig S (2004) EEGLAB: An open source toolbox for analysis of
922 single-trial EEG dynamics including independent component analysis. J
923 Neurosci Meth 134:9–21. http://doi.org/10.1016/j.jneumeth.2003.10.009

924 Ditterich J (2006) Evidence for time-variant decision making. Eur J Neurosci,
925 24:3628–41. http://doi.org/https://doi.org/10.1111/j.1460-9568.2006.05221.x

926 Dmochowski JP, Norcia AM (2015) Cortical components of reaction-time during
927 perceptual decisions in humans. PLoS ONE 10:1–18.
928 http://doi.org/10.1371/journal.pone.0143339

929 Donkin C, Brown SD, Heathcote A (2009) The overconstraint of response time
930 models: Rethinking the scaling problem. Psychon B Rev 16:1129–1135.
931 http://doi.org/10.3758/PBR.16.6.1129

Donkin C, Brown S, Heathcote A, Wagenmakers E (2011) Diffusion versus linear ballistic accumulation: different models but the same conclusions about psychological processes? Psychon B Rev 18:61–69. http://doi.org/10.3758/s13423-010-0022-4

Donkin C, Heathcote A, Brown S (2009) Is the Linear Ballistic Accumulator Model Really the Simplest Model of Choice Response Times: A Bayesian Model Complexity Analysis. In 9th International Conference on Cognitive Modeling—ICCM2009 (Manchester, UK).

Donner TH, Siegel M, Fries P, Engel AK (2009) Buildup of Choice-Predictive Activity in Human Motor Cortex during Perceptual Decision Making. Curr Biol 19:1581–1585. http://doi.org/10.1016/j.cub.2009.07.066

Duque J, Greenhouse I, Labruna L, Ivry RB (2017) Physiological Markers of Motor Inhibition during Human Behavior. Trends Neurosci 40:219–236. http://doi.org/10.1016/j.tins.2017.02.006

Duque J, Lew D, Mazzocchio R, Olivier E, Ivry RB (2010) Evidence for Two Concurrent Inhibitory Mechanisms during Response Preparation. J Neurosci 30:3793–3802. http://doi.org/10.1523/JNEUROSCI.5722-09.2010

Evans NJ, Hawkins GE, Boehm U, Wagenmakers EJ, Brown SD (2017) The computations that support simple decision-making: A comparison between the diffusion and urgency-gating models. Sci Rep 7:1–13. http://doi.org/10.1038/s41598-017-16694-7

Gold JI, Shadlen MN (2000) Representation of a perceptual decision in developing oculomotor commands. Nature 404:390–394. http://doi.org/10.1038/35006062

955 Groppe DM, Urbach TP, Kutas M (2011) Mass univariate analysis of event-related
956 brain potentials/fields I: A critical tutorial review. Psychophysiology 48:1711–
957 1725. http://doi.org/10.1111/j.1469-8986.2011.01273.x

958 Hadar A, Rowe P, Di Costa S, Jones A, Yarrow K (2016) Motor-evoked potentials
959 reveal a motor-cortical readout of evidence accumulation for sensorimotor
960 decisions. Psychophysiology 53:1721-1731.doi: 10.1111/psyp.12737

961 Hanks TD, Kiani R, Shadlen MN (2014) A neural mechanism of speed-accuracy
962 tradeoff in macaque area LIP. eLife 27:1–17. http://doi.org/10.7554/eLife.02260

963 Hawkins GE, Forstmann BU, Wagenmakers EJ, Ratcliff R, Brown SD (2015)
964 Revisiting the evidence for collapsing boundaries and urgency signals in
965 perceptual decision-making. J Neurosci 35:2476–84.
966 http://doi.org/10.1523/JNEUROSCI.2410-14.2015

967 Hawkins GE, Wagenmakers EJ, Ratcliff R, Brown SD (2015) Discriminating
968 evidence accumulation from urgency signals in speeded decision making. J
969 Neurophysiol 114:40-47. http://doi.org/10.1152/jn.00088.2015

970 Heathcote A, Brown S, Mewhort DJK (2002) Quantile maximum likelihood estimation
971 of response time distributions. Psychon B Rev 9:1–31.
972 http://doi.org/10.3758/BF03196299

973 Heitz RP (2014) The speed-accuracy tradeoff: History, physiology, methodology, and
974 behavior. Front Neurosci 8:1–19. http://doi.org/10.3389/fnins.2014.00150

975 Heitz RP, Schall JD (2012) Neural Mechanisms of Speed-Accuracy Tradeoff. Neuron
976 76:616–628. http://doi.org/10.1016/j.neuron.2012.08.030

977 Heitz RP, Schall JD (2013) Neural chronometry and coherency across speed-
978 accuracy demands reveal lack of homomorphism between computational and
979 neural mechanisms of evidence accumulation. Philos T Roy Soc B
980 368:20130071. http://doi.org/10.1098/rstb.2013.0071

981 Hick WE (1952) On the rate of gain of information. Q J Exp Psychol 4:11–26.
982 http://doi.org/10.1016/0022-0965(78)90002-4

983 Ivanoff J, Branning P, Marois R (2008) fMRI evidence for a dual process account of
984 the speed-accuracy tradeoff in decision-making. PLoS ONE 3.
985 http://doi.org/10.1371/journal.pone.0002635

986 Karsilar H, Simen P, Papadakis S, Balci F (2014) Speed accuracy trade-off under
987 response deadlines. Front Neurosci 8:1–18.
988 http://doi.org/10.3389/fnins.2014.00248

989 Kayser J, Tenke CE (2006) Principal components analysis of Laplacian waveforms
990 as a generic method for identifying ERP generator patterns: II. Adequacy of low-
991 density estimates. Clin Neurophysiol 117:369–380.
992 http://doi.org/10.1016/j.clinph.2005.08.033

993 Kelly SP, O'Connell RG (2013) Internal and external influences on the rate of
994 sensory evidence accumulation in the human brain. J Neurosci 33:19434–
995 19441. http://doi.org/10.1523/JNEUROSCI.3355-13.2013

996 Klein-Flugge MC, Bestmann S (2012) Time-Dependent Changes in Human
997 Corticospinal Excitability Reveal Value-Based Competition for Action during
998 Decision Processing. J Neurosci 32:8373–8382.
999 http://doi.org/10.1523/JNEUROSCI.0270-12.2012

1000 Kleiner M, Brainard DH, Pelli DG, Broussard C, Wolf T, Niehorster D (2007) What's
1001 new in Psychtoolbox-3? Perception 36. http://doi.org/10.1068/v070821

1002 Laberge D (1962) A recruitment theory of simple behavior. Psychometrika 27:375–
1003 396.

1004 Lagarias JC, Reeds JA, Wright MH, Wright PE (1998) Convergence Properties of the
1005 Nelder-Mead Simplex Method in Low Dimensions. SIAM J Optimiz 9:112–147.
1006 http://doi.org/10.1137/S1052623496303470

1007 Luce RD (1986) Response Times: Their Role in Inferring Elementary Mental
1008 Organization. New York: Oxford University Press.

1009 Milosavljevic M, Malmaud J, Huth A (2010) The Drift Diffusion Model can account for
1010 the accuracy and reaction time of value-based choices under high and low time
1011 pressure. Judgem Decis Mak 5:437–449. http://doi.org/10.2139/ssrn.1901533

1012 Mulder MJ, van Maanen L, Forstmann BU (2014) Perceptual decision neurosciences
1013 - a model-based review. Neuroscience 277:872–884.
1014 http://doi.org/10.1016/j.neuroscience.2014.07.031

1015 Murphy PR, Boonstra E, Nieuwenhuis S (2016) Global gain modulation generates
1016 time-dependent urgency during perceptual choice in humans. Nat Commun
1017 7:13526. http://doi.org/10.1038/ncomms13526

1018 Nichols TE, Holmes AP (2001) Nonparametric Permutation Tests for {PET}
1019 functional Neuroimaging Experiments: A Primer with examples. Hum Brain
1020 Mapp 15:1–25. http://doi.org/10.1002/hbm.1058

1021 O'Connell RG, Dockree PM, Kelly SP (2012) A supramodal accumulation-to-bound
1022 signal that determines perceptual decisions in humans. Nat Neurosci 15:1729–
1023 35. http://doi.org/10.1038/nn.3248

1024 Pelli DG (1997) The VideoToolbox software for visual psychophysics: transforming
1025 numbers into movies. Spatial Vision. http://doi.org/10.1163/156856897X00366

1026 Price KV, Storn RM, Jouni LA (2005). Differential Evolution: A Practical Approach to
1027 Global Optimization. Heidelberg: Springer Berlin Heidelberg.
1028 http://doi.org/10.1038/155531c0

1029 Ratcliff R (1978). A theory of memory retrieval. Psychol Rev 85:59–108.
1030 http://doi.org/10.1037/0033-295X.85.2.59

1031 Ratcliff R, McKoon G (2008) The diffusion decision model: theory and data for two-
1032 choice decision tasks. Neural Comput 20:873–922.
1033 http://doi.org/10.1162/neco.2008.12-06-420

1034 Ratcliff R, Rouder JN (1998) Modeling Response Times for Two-Choice Decisions.
1035 Psychol Sci 9:347–356.

1036 Ratcliff R, Thapar A, McKoon G (2003) A diffusion model analysis of the effects of
1037 aging on brightness discrimination. Percept Psychophys 65:523–35.
1038 http://doi.org/10.3758/BF03194580

1039 Ratcliff R, Thapar A, McKoon G (2004) A diffusion model analysis of the effects of
1040 aging on recognition memory. J Mem Lang 50:408–424.
1041 http://doi.org/10.1016/j.jml.2003.11.002

1042 Resulaj A, Kiani R, Wolpert DM, Shadlen MN (2009) Changes of mind in decision-
1043 making. Nature 461:263–266. http://doi.org/10.1038/nature08275

1044 Roitman JD, Shadlen MN (2002) Response of neurons in the lateral intraparietal
1045 area during a combined visual discrimination reaction time task. J Neurosci
1046 22:9475–9489. http://doi.org/10.1016/S0377-2217(02)00363-6

1047 Shadlen MN, Newsome WT (1996) Motion perception: seeing and deciding. P Natl
1048 Acad Sci USA 93:628–633. http://doi.org/10.1073/pnas.93.2.628

1049 Shadlen MN, Newsome WT (2001) Neural Basis of a Perceptual Decision in the
1050 Parietal Cortex (Area LIP) of the Rhesus Monkey. J Neurophysiol 86:1916–
1051 1936.

1052 Smith PL, Ratcliff R (2004) Psychology and neurobiology of simple decisions. Trends
1053 Neurosci 27:161–168. http://doi.org/10.1016/j.tins.2004.01.006

1054 Thura D, Beauregard-Racine J, Fradet CW, Cisek P (2012) Decision making by
1055 urgency gating: theory and experimental support. J Neurophysiol 108:2912–
1056 2930. http://doi.org/10.1152/jn.01071.2011

1057 Thura D, Cisek P (2017) The Basal Ganglia Do Not Select Reach Targets but
1058 Control the Urgency of Commitment. Neuron 95:1160–1170.
1059 http://doi.org/10.1016/j.neuron.2017.07.039

1060 Twomey DM, Kelly SP, O'Connell RG (2016) Abstract and Effector-Selective
1061 Decision Signals Exhibit Qualitatively Distinct Dynamics before Delayed
1062 Perceptual Reports. J Neurosci 36:7346–7352.
1063 http://doi.org/10.1523/JNEUROSCI.4162-15.2016

1064 Twomey DM, Murphy PR, Kelly SP, O'Connell RG (2015) The classic P300 encodes
1065 a build-to-threshold decision variable. Eur J Neurosci 42:1636–1643.
1066 http://doi.org/10.1111/ejn.12936

1067 Usher M, McClelland JL (2001) The time course of perceptual choice: The leaky,
1068 competing accumulator model. Psychol Rev 108:550–592.
1069 http://doi.org/10.1037/0033-295X.108.3.550

1070 Vickers D (1970) Evidence for an Accumulator Model of Psychophysical
1071 Discrimination. Ergonomics 13:37–58.
1072 http://doi.org/https://doi.org/10.1080/00140137008931117

1073 Watson AP, Pelli DG (1983) QUEST: A Bayesian adaptive psychometric method.
1074 Percept Psychophys 33:113–120.

1075 Wickelgren WA (1977) Speed-Accuracy Tradeoff and Information Processing
1076 Dynamics. Acta Psychol 41:67–85.

1077

Table Legends

Table 1: Model Comparison: BIC and AIC values for each model and each experiment (best BIC and AIC values in bold).The terms "fixed" and "free" here relate specifically to changes across speed/accuracy instructions, as accumulation rate (V) was always free to vary between difficulty conditions.

1084 Table 2: Estimated parameter values for the best-supported model (Model 2) when
1085 expressed with both free and forced-excursion in both experiments. The response
1086 boundary A in the 'accuracy' condition was set to 1 as a scaling parameter.
1087 Parameters are not comparable across experiments, as the TMS fit is to data
1088 normalised to the median RT of each participant.

Figure Captions

Figure 1: TMS experiment procedure: a) random dot motion task: after a fixation cross and a period of random motion, coherent motion (here: upward, coherence 70%) is displayed for 2000 ms or until response (the same task was used in the EEG experiment); b) response setup in TMS experiment: Participants held one button (up) between their thumb and index finger (pinch) and one in the palm of their hand (down), attached to a cylinder (grasp); EMG electrodes were placed on the ADM and FDI; c) example EMG traces from a single trial (here, a hard speed trial, where the responding muscle is the FDI and the non-responding muscle is the ADM); d) To create model predictions which are comparable to MEP data, accumulation values from both the correct accumulator (corresponding to the responding muscle) and the incorrect accumulator (corresponding to the non-responding muscle) are sampled at simulated TMS times; e) Illustrative real MEP amplitudes (from the speed/easy condition) collated from all participants; f) MEPs and simulations (not shown) are then z-scored per muscle, participant, and session (note that latencies were normalised by the median, not maximum, EMG RT for each participant); g) real and simulated continuous signals can be created for each muscle (responding, non-responding), using a Gaussian smoothing kernel; h) however, to remove non-specific processes, the same smoothing is applied to the difference between simultaneously recorded MEPs (responding minus non-responding).

Figure 2: Behavioural results for both the TMS experiment (a) and the EEG experiment (b): reaction time (left) and accuracy scores (right) for each condition. Top left panel shows both EMG RT (bars) and button RT (dashed lines). Error bars indicate 95% Confidence Interval. ** indicates $p < .001$.

Figure 3: Neural and modelling results: Top: neural data; Bottom: model comparison; Left: TMS experiment; Right: EEG experiment; a) stimulus-locked (left) and response-locked (right) MEP signal for each condition. Each panel shows both the MEP signal associated with the responding muscle (dark) and the non-responding muscle (light). Shaded areas indicate 95% confidence intervals; b) CPP: stimulus-locked (left) and response-locked (right) CPP waveform for each condition. The bottom right of the panel shows the topography of the ERP, averaged over the stimulus-locked time interval of 0 to 1000 ms. Electrodes used to generate CPP waveforms are highlighted; c) stimulus-locked (left) and response-locked (right) MEP-average signal (responding minus non-responding muscle); d) stimulus-locked (left) and response-locked (right) model predictions made by the free-excursion variant of the best-supported model; e) stimulus-locked (left) and response-locked (right) model predictions made by the forced-excursion variant of the best-supported model; f) stimulus-locked (left) and response-locked (right) CPP; note that the CPP here is a pooled average rather than a grand average and therefore differs from b. Additionally, the waveform has been low-pass filtered with a cut-off of 5 Hz to assist comparison with model predictions; f) stimulus-locked (left) and response-locked (right) model predictions (correct and incorrect accumulator summed) made by the free-excursion variant of the best-supported model; g) stimulus-locked (left) and response-locked (right) model predictions (correct and incorrect accumulator summed) made by the forced-excursion variant of the best-supported model.

Figure 4: Model fit for the TMS experiment (a) and the EEG experiment (b): quantiles estimated from behavioural data (circles) and Model 2 simulations (crosses and lines) for easy (top) and hard (bottom) decisions. For each condition, correct (thick) and incorrect (thin) quantiles are displayed separately. Note that the model fit is identical for the forced-excursion and the standard free-excursion race model.

Model Number	A	S_z	$v_{correct}$	$v_{incorrect}$	T_{er}	S_{Ter}	σ	Number of parameters	TMS Experiment		EEG Experiment	
									AIC	BIC	AIC	BIC
Model 1	free	fixed	fixed	fixed	fixed	fixed	fixed	9	44,868	44,933	62,398	62,466
Model 2	free	free	fixed	fixed	fixed	fixed	fixed	10	**44,859**	**44,932**	**62,389**	**62,464**
Model 3	free	fixed	fixed	fixed	free	fixed	fixed	10	44,865	44,937	62,404	62,479

Parameters		TMS Experiment				EEG Experiment			
		Free-excursion		Forced-excursion		Free-excursion		Forced-excursion	
		accuracy	speed	accuracy	speed	accuracy	speed	accuracy	speed
S_Z		0.447	0.523	0.447	0.586	0.319	0.541	0.319	0.664
A		1	0.893	1		1	0.815	1	
T_{er}		0.382		0.382		0.257		0.257	
S_{Ter}		0.374		0.374		0.229		0.229	
σ^2		0.499		0.499	0.558	0.785		0.785	0.964
$v_{correct}$	*easy*	1.280		1.28	1.433	2.475		2.475	3.038
	hard	0.634		0.634	0.710	1.350		1.350	1.656
$v_{incorrect}$	*easy*	0.098		0.098	0.109	0.253		0.253	0.310
	hard	0.004		0.004	0.005	0.054		0.054	0.066

a) Random dot motion task

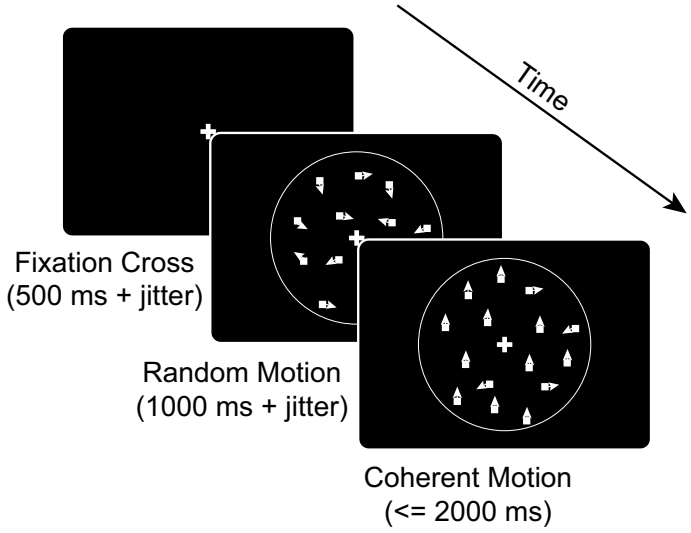

b) Response/EMG setup

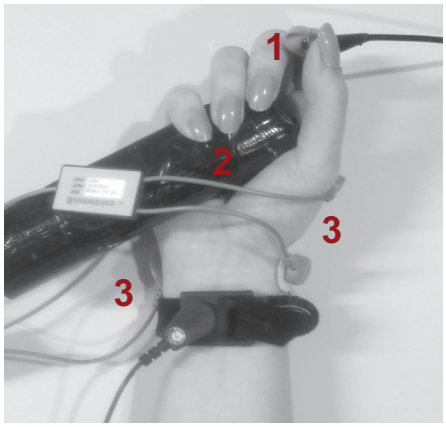

1 'Pinch' response button
2 'Grasp' response button
3 EMG electrodes

c) MEP recording

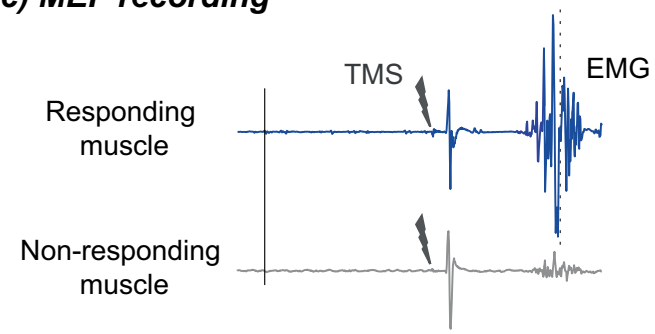

d) MEP simulation

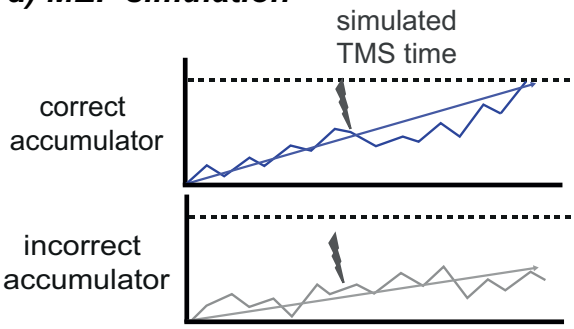

e) MEP amplitudes: raw data

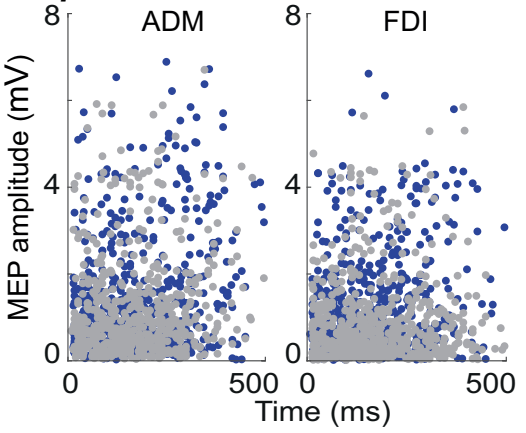

f) MEP amplitudes: normalised

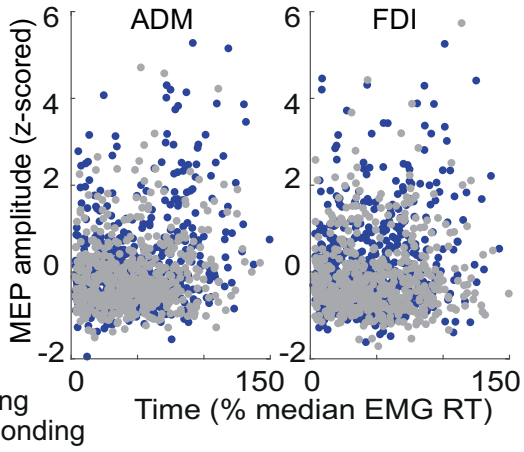

g) MEP smoothing

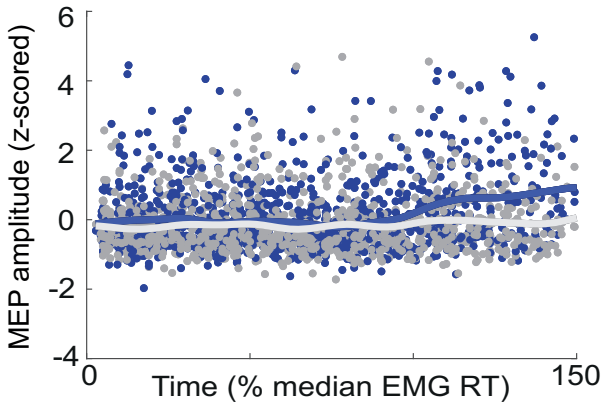

h) MEP subtraction